



Tailoring the solar absorptivity of thermochromic material $\text{La}_{0.7}\text{Ca}_{0.2}\text{Sr}_{0.1}\text{MnO}_3$

Desong Fan, Qiang Li*, Yimin Xuan

School of Energy and Power Engineering, Nanjing University of Science and Technology, Nanjing, Jiangsu 210094, PR China

ARTICLE INFO

Article history:

Received 27 April 2011

Received in revised form

22 July 2011

Accepted 9 August 2011

Available online 16 August 2011

Keywords:

Simulated annealing genetic algorithm

Thermochromic material

Optical thin film

Solar absorptivity

Optical constants

Emissivity

ABSTRACT

$\text{La}_{0.7}\text{Ca}_{0.2}\text{Sr}_{0.1}\text{MnO}_3$ is a thermochromic material which can be used as thermal control device. However, its solar absorptivity is too high for that in spacecraft application. To reduce its solar absorptivity, an optical thin film is designed in this paper by using simulated annealing genetic algorithm. This film can effectively reflect the solar radiation at the short wave and can be transparent at long wave. A designed optical thin film is deposited on the surface of thermochromic material by electron beam evaporation. Experiments show that the solar absorptivity is reduced from 0.78 to 0.28 at short wave, and the transmissivity is 0.87 at long wave. The results match pretty well with the theoretical predictions in a global view.

© 2011 Elsevier Ltd. All rights reserved.

1. Introduction

Thermochromic materials have received much attention for space applications for their thermochromic properties induced by metal–insulator transition. For example, VO_2 is used as thermal switches in satellites [1]; $\text{Sm}_{1-x}\text{Ca}_x\text{MnO}_3$ shows great prospect in thermochromic switch [2]; $\text{La}_{1-x}\text{Sr}_x\text{MnO}_3$ can be developed as a thermal control material [3,4]. Perovskite-type manganese oxide $\text{La}_{0.7}\text{Ca}_{0.2}\text{Sr}_{0.1}\text{MnO}_3$ (LCSMO) is promising for thermochromic materials because its emissivity can be changed automatically with temperature in our previous work [5]. Experiments prove that the emissivity of LCSMO can reach a high value of 0.62 at 350 K and a low value of 0.39 at 243 K. The range of variation is 0.23, which is suitable for application of thermal control in spacecraft. However, from the viewpoint of practical application in spacecraft, its solar absorptivity have a value of 0.78,

which is too large that the temperature of surface will be too high if exposed to solar radiation.

Generally, the surface temperature of a spacecraft is governed by the heat dissipation inside spacecraft, the heat input from the sun, the reflected solar energy and infrared radiation from the earth. When a thermochromic material integrated surface of a spacecraft is exposed to a harsh thermal environment, its temperature will increase rapidly beyond the permissible working temperature. In order to solve this problem, we design an optical thin film on the top of the thermochromic material. This film can effectively reflect the solar radiation in the wavelength region from 0.25 to 2.5 μm and can be transparent above 2.5 μm . By this means, the surface temperature of a spacecraft can be controlled effectively.

2. Characteristics of $\text{La}_{0.7}\text{Ca}_{0.2}\text{Sr}_{0.1}\text{MnO}_3$

Thermochromic material $\text{La}_{0.7}\text{Ca}_{0.2}\text{Sr}_{0.1}\text{MnO}_3$ is synthesized by conventional solid-state reaction method [5]. Its crystal structure is characterized by X-ray diffraction (XRD) (D8 ADVANCE, Bruker Co., Germany) with $\text{Cu-K}\alpha$

* Corresponding author. Tel.: +86 25 84315488.

E-mail address: liqiang@mail.njust.edu.cn (Q. Li).

radiation at room temperature. Its spectral characteristics are obtained by using an ultraviolet–visible–near infrared spectrophotometer (Cary5000, Varian Co., America) and a FT-IR spectrometer (VERTEX80v, Bruker Co., Germany; NEXUS670, Varian Co., America). The wavelength resolution of Cary5000 is 0.05 nm in the ultraviolet–visible region and 0.2 nm in the near infrared region, respectively. The resolution of VERTEX80v and NEXUS670 is 0.07 cm^{-1} and 0.09 cm^{-1} , respectively. The near-normal reflectivity (incident angle of 15°) is measured by using the Transmission-Reflection Dewar of VERTEX80v between 0.78 and $20\text{ }\mu\text{m}$ with temperature and by using the NEXUS670 above $20\text{ }\mu\text{m}$. The solar absorptivity is determined by measuring a spectral variation in $0.25\text{--}2.5\text{ }\mu\text{m}$ region using an integrating sphere at room temperature. Surface roughness of the polished surface is measured by an atomic force microscope (CSPM4000, Being Ltd., Beijing in China). The lateral resolution of the AFM is 0.26 nm and the vertical one is 0.1 nm .

The XRD pattern of LCSMO in Fig. 1 shows a characteristic of single phase with perovskite-type structure. All reflections can be indexed on the basis of the $Pnma$ orthorhombic space group. The inset image in Fig. 1 indicates that the lattice structure of LCSMO is distorted.

The measured near-normal reflectivity (incident angle of 15°) of LCSMO is shown in Fig. 2. It can be seen that the reflectivity shows a large variation with temperature at wavelength above $2.5\text{ }\mu\text{m}$. As the temperature increases, the reflectivity at long wavelength gradually decreases. The reflectivity at low temperature is higher than which at high temperature. This reveals that the reflectivity shows a transition of metal–insulator with temperature. The reflection peak, which around $4.2\text{ }\mu\text{m}$ at various temperatures is a interference of carbon dioxide in ambient air.

The solar absorptivity is calculated by using the near-normal spectral reflectivity data at 293 K over the wavelength region of $0.25\text{--}2.5\text{ }\mu\text{m}$ in the inset of Fig. 2. It is 0.78 , which is too large to reject excess heat from LCSMO surface exposed to harsh space environment.

Fig. 3 shows the emissivity of LCSMO at various temperatures from 243 K to 350 K . It is obvious that the emissivity of LCSMO increases with temperature and has a significantly rise in the vicinity of transition

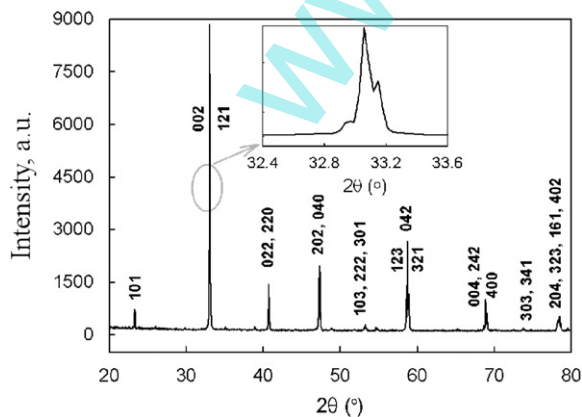


Fig. 1. XRD pattern of $\text{La}_{0.7}\text{Ca}_{0.2}\text{Sr}_{0.1}\text{MnO}_3$.

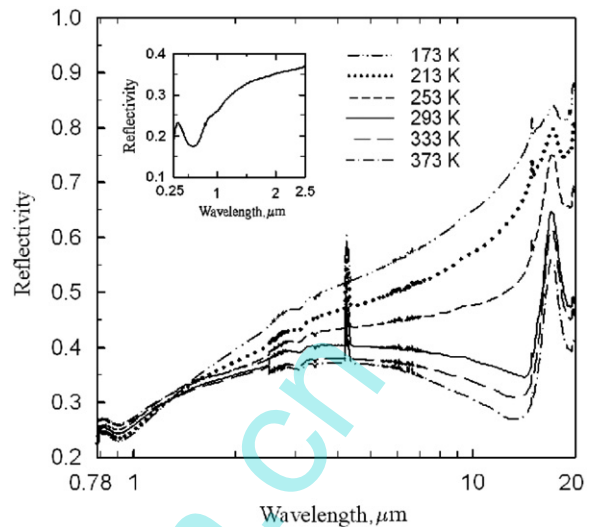


Fig. 2. Spectral reflectivity of $\text{La}_{0.7}\text{Ca}_{0.2}\text{Sr}_{0.1}\text{MnO}_3$ at various temperatures in the wavelength region of $0.78\text{--}20\text{ }\mu\text{m}$. The inset shows the spectral reflectivity at 293 K in the wavelength region of $0.25\text{--}2.5\text{ }\mu\text{m}$.

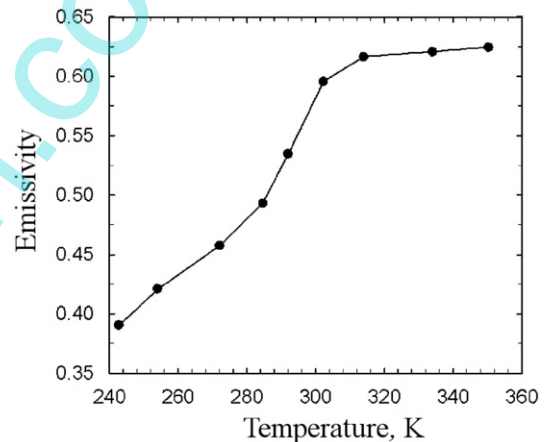


Fig. 3. Temperature dependence of the emissivity of $\text{La}_{0.7}\text{Ca}_{0.2}\text{Sr}_{0.1}\text{MnO}_3$.

temperature $T_p=293\text{ K}$. Similar to the spectral reflectivity (Fig. 2), the emissivity also shows a transition from metal state to insulator state with temperature. This is a strong coupling between the optical and the thermal processes.

The surface of LCSMO is polished since a smooth surface can decrease the trapping of incident radiation, thereby decreasing its emissivity below transition temperature [6,3]. The root-mean-square roughness, which is accessed from AFM, is about 6 nm . The AFM image, in Fig. 4, shows that the LCSMO surface is dense and uniform. No cracks or defects have been observed.

3. Calculation method for solar absorptivity of film system

In this section, the solar absorptivity of a film system which contains thin film and a LCSMO substrate is

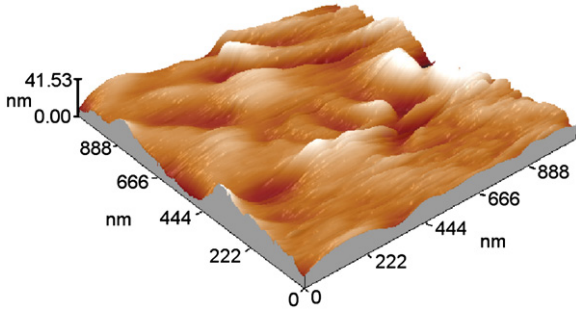


Fig. 4. Three-dimension AFM image of $\text{La}_{0.7}\text{Ca}_{0.2}\text{Sr}_{0.1}\text{MnO}_3$.

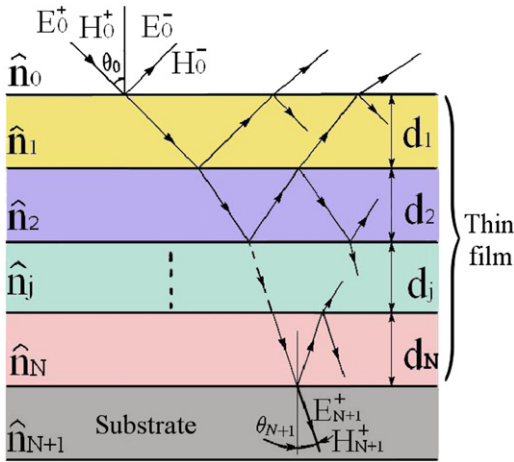


Fig. 5. Structure of film system.

deduced from its spectral reflectivity. The structure of the film system is shown in Fig. 5. The spectral reflectivity is calculated by using a characteristic matrix method [7]. When the interference is taken into consideration, the characteristic matrix of a film system which contains multiple reflections at the boundary surface between j th and $j+1$ th layers can be expressed as

$$\begin{bmatrix} B \\ C \end{bmatrix} = \left\{ \prod_{j=1}^N \begin{bmatrix} \cos \delta_j & i \sin \delta_j / \eta_j \\ i \eta_j \sin \delta_j & \cos \delta_j \end{bmatrix} \right\} \begin{bmatrix} 1 \\ \eta_{N+1} \end{bmatrix}, \quad (1)$$

where $\delta_k = 2\pi \hat{n}_k d_k \cos \theta_j / \lambda$, θ_j is the incident angle of the electromagnetic wave, d_j is the geometric thickness, \hat{n}_j is the complex refractive index of the j th layer, N is the total number of layers, η_{N+1} is the optical admittance of substrate medium, and λ is the wavelength of incident wave. η_j is defined in two polarization modes as

$$\eta_j = \begin{cases} n_j \cos \theta_j & \text{for s-waves,} \\ n_j / \cos \theta_j & \text{for p-waves.} \end{cases} \quad (2)$$

If the incident angle of an air layer θ_0 (in Fig. 5) is given, the $\cos \theta_j$ can be obtained from Snell's law. Thus, the spectral reflectivity $R(\lambda, \theta)$ as a function of incident angle θ and wavelength λ is expressed as

$$R(\lambda, \theta) = \frac{R'_s(\lambda, \theta) + R'_p(\lambda, \theta)}{2} \quad (3)$$

and

$$R'(\lambda, \theta) = \left| \frac{\eta_0 B - C}{\eta_0 B + C} \right|^2. \quad (4)$$

where η_0 denotes the optical admittance of air layer.

For thermochromic materials, the solar absorptivity of the film system can be calculated by as equation as follows [8]:

$$\alpha_s(\theta) = \frac{\int_{0.25}^{2.5} [1 - R(\lambda, \theta)] I_s(\lambda) d\lambda}{\int_{0.25}^{2.5} I_s(\lambda) d\lambda}, \quad (5)$$

where $R(\lambda, \theta)$ denotes the reflectivity of film system in the wavelength region of 0.25–2.5 μm , and $I_s(\lambda)$ is the solar radiation intensity [9]. In the wavelength range of 0.25–2.5 μm , it contains about 96% of the solar radiation intensity at room temperature.

4. Optical constants of $\text{La}_{0.7}\text{Ca}_{0.2}\text{Sr}_{0.1}\text{MnO}_3$

In order to calculate the spectral reflectivity of a film system, the optical constants of LCSMO should be known. In the 0.25–2.0 μm region, it is measured by ellipsometry at room temperature as shown in Fig. 6. However, at the wavelength above 2.0 μm , the data has not been obtained for technical limitation. As an alternatively way, the optical constants are also calculated by K–K analysis using a measured near-normal reflectivity in 0.25–100 μm region. The calculated results are illustrated in Fig. 7. Comparing with the measured optical constant in the wavelength region of 0.25–2 μm , the refractive index from K–K analysis is larger, and the extinction coefficient is smaller. This difference may be attributed to the usage of near-normal (incidence angle of 15°) spectral reflectivity in K–K analysis. In this paper, the optical constant in 0.25–2.0 μm region is selected from experimental measurement and which above 2.0 μm is selected from calculation value. The refractive index n and extinction coefficient k are given by

$$n = \frac{1 - R}{1 + R - 2\sqrt{R} \cos \theta} \quad (6)$$

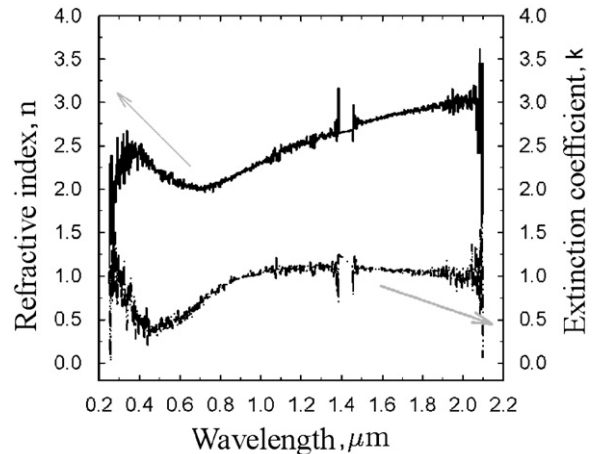


Fig. 6. Measured optical constants of $\text{La}_{0.7}\text{Ca}_{0.2}\text{Sr}_{0.1}\text{MnO}_3$ at room temperature.

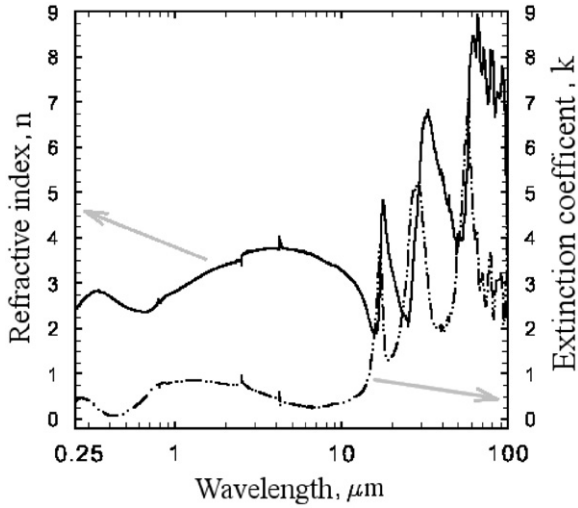


Fig. 7. Calculated optical constants of $\text{La}_{0.7}\text{Ca}_{0.2}\text{Sr}_{0.1}\text{MnO}_3$ from K-K analysis.

and

$$k = \frac{-2\sqrt{R} \sin \theta}{1 + R - 2\sqrt{R} \cos \theta}. \quad (7)$$

where R is the measured spectral reflectance of LCSMO. The parameter θ represents phase shift, which is a function of frequency. It can be defined as

$$\theta(\omega) = \frac{\omega}{\pi} \int_0^\infty \frac{\ln R(\omega') - \ln R(\omega)}{\omega^2 - \omega'^2} d\omega'. \quad (8)$$

In the wavelength region of 0.25–100 μm , the $R(\omega)$ is obtained from experiments. Above 100 μm , the $R(\omega)$ is treated as a constant. Additionally, the reflectivity $R(\omega)$ is treated as a constant in the wavelength region of 0.1–0.25 μm , and as the exponential extrapolation ($R \propto \omega^{-4}$) at the wavelength below 0.1 μm [10].

5. Design principle and method of optical thin film

The design of optical thin film is basically an optimization problem. The objective is to minimize the deviation between the actual spectral characteristics and the target spectral characteristics of film system by adjusting the film structures including the complex refractive index of film materials and film thickness. Therefore, it is necessary to construct an evaluation function which describes the relationship between the deviation and the film structures. A numerical method is then followed for the optimal solution of evaluation function.

Traditional thin film design methods (gradient, damped least squares method) always need a good initial thin film structure. A computer is then employed to adjust the structures of thin film to achieve its desired performance. However, these methods hardly meets the multiple-layer systems. Moreover, they can only get a local convergence value near the initial structure. If the initial structure is far from optimal solution, it is hard to obtain the desired solution. To overcome these shortcomings, the genetic algorithm (GA), which is a highly efficient

stochastic search algorithm [11], is introduced. It has been successfully applied to optical thin film designs [12–14]. GA is different from the traditional design methods in many ways. Firstly, it searches for the optimum solutions through a population of solutions instead of a single solution [15]. Secondly, GA shows a special interest in the field of optical thin film design that it can incorporate both continuous optimization variables (such as the film thickness) and discrete variables (such as the selection of film materials). Finally, GA does not need a good initial structure to ensure convergence because it would not be easily trapped in a local optimum.

In the design process, a simulated annealing genetic algorithm (SAGA) based on the genetic algorithm (GA) and simulated annealing (SA) is employed in this paper. SAGA inherits the advantage of GA, and its selection space of population is enlarged by introducing the SA. In this algorithm, the search space and its coded strings is established. These coded strings determine the structure of each individual. An initial population, which contains an appropriate number of individuals, is created at random. Each individual is assigned a fitness value. A new population is produced from the old population by genetic operations, i.e., selection, crossover and mutation.

In the present study, the variable search space (the film thickness and film material of each layer) in our optimization problem is a $2N$ dimensional parameter, where N is the number of layers in the film system. An individual \mathbb{X} can be expressed as a $2N$ dimensional vector $\mathbb{X} = (d_1, \hat{n}_1, \dots, d_i, \hat{n}_i, \dots, d_n, \hat{n}_n)$, where d_i and \hat{n}_i represent the thickness and the complex refractive index of i th layer, respectively. The search space can be written as $[\mathbb{U}, \mathbb{V}]^N$, where $\mathbb{U} = [d_{\min}, d_{\max}]^N$ and $\mathbb{V} = [\hat{n}_1, \hat{n}_2, \dots, \hat{n}_p]^N$, where $P \leq N$. Vector \mathbb{V} is a discrete space including the complex refractive index of available materials. The search space $[\mathbb{U}, \mathbb{V}]^N$ is determined before the running of program. The geometric thickness of each layer is set as $\mathbb{U} = [0, 400]^N$ and is coded with real number. The maximum number of the layers is set to 10 which is large enough to make sure that the solar absorptivity can be reduced to the desired value, and is small enough to obtain a transparent film structure at the wavelength above 2.5 μm . The available materials for film include ZnS, ZnSe, MgF_2 , Si and Ge. These materials are mapped to integer numbers. Comparing with the metal, these dielectric and semiconductor materials can provide a lower absorption loss and a higher reflectivity. Furthermore, these materials are common infrared-transparent materials. For the optical constants of these materials, the data including dispersion and absorption is obtained from the literatures [16,17].

In this paragraph, the optical properties of film materials are clarified during the calculation. The extinction coefficient of MgF_2 is neglected in the wavelength range of 0.25–10 μm because the material is transparent in this spectral region. In 10–100 μm region, the extinction coefficient of MgF_2 varying with the wavelength is considered since the absorption loss of MgF_2 is considerable. The wavelength-dependent refractive index of MgF_2 is used over the wavelength range of 0.25–100 μm . For germanium, its wavelength-dependent extinction

coefficient covers a wavelength range from 0.25 to 100 μm ; its refractive index is a function of wavelength in 0.25–4 μm and is treated as a constant at the wavelength above 4 μm . For silicon, its refractive index varies with the wavelength in 0.25–3 μm and is a constant of 3.4 over the wavelength range 3–100 μm ; its extinction coefficient is a function of wavelength below 1 μm and is assumed as zero above 1 μm because of a sufficiently small value [16].

To simplify calculation, a normal incident light from an air layer is considered in this work. The population size is 30 and the maximum iteration generation is 3000. The genetic operation of the selection simulated annealing [18] and the adaptive crossover and mutation [11] is utilized. The probabilities of crossover and mutation vary with the fitness values of solutions. In this process, it is advantageous that the high fitness values are protected and the values with subaverage fitness are totally disrupted.

To evaluate the performance of each individual, the evaluation function F that determines the fitness of each individual, and the fitness function Fit are respectively defined as

$$F = \left(\frac{\alpha_s - \hat{\alpha}_s}{\delta\alpha_s} \right)^2 + \left\{ \int_{2.5}^{100} [R(\lambda, \theta) - \hat{R}]^2 d\lambda \right\}^{1/2} \quad (9)$$

and

$$Fit = 1/F, \quad (10)$$

where $\delta\alpha_s$ is a tolerance factor ($\delta\alpha_s = 0.01$), $\hat{\alpha}_s$ and \hat{R} are the target values of solar absorptivity and of spectral reflectivity of film system above 2.5 μm , respectively. $R(\lambda, \theta)$ and α_s are calculated from Eqs. (3) and (5). The spectral region (2.5–100 μm) contains approximately 99% of radiative power from the surface of film system at room temperature.

6. Results and discussion

The measured α_s of LCSMO is 0.78 in the present study which is too high. In order to decline the solar radiation to the surface of LCSMO in spacecraft application, we develop a film system, which has a small solar absorptivity in 0.25–2.5 μm region and is transparent in 2.5–100 μm region, using a SAGA. In this algorithm, the target absorptivity $\hat{\alpha}_s$ is set to 0.2. The absorptivity is expected to become as small as possible. However, if the absorptivity is too smaller, it is difficult to ensure a transparent structure in such wide region from 2.5 to 100 μm simultaneously. The target reflectivity \hat{R} is set to zero to ensure a transparent structure beyond the wavelength of 2.5 μm .

The evaluation values of evaluation function of the best individual in SAGA are shown in Fig. 8. The evaluation, that is the number of individuals which can reach goal, is rapidly decreasing before the tenth generation. A good individual suddenly appeared at around 400th generation, though the variation of evaluation value is smooth from the tenth generation to the last one. The individual with the maximum fitness values which are

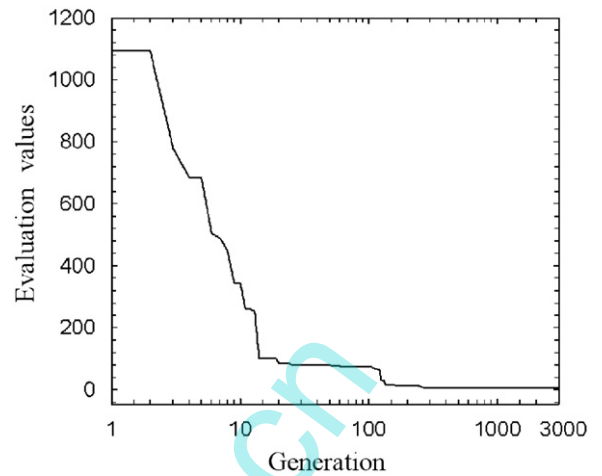


Fig. 8. The evaluation values of the best individual in SAGA.

Table 1
Optimal solution of film system obtained by the SAGA.

Layer number	Material	Thickness (nm)
1	Si	24
2	MgF ₂	125
3	Si	36
4	MgF ₂	160
5	Si	37
6	MgF ₂	163
7	Ge	96
8	MgF ₂	172
9 ^a	Ge	125

^a The ninth layer is situated on the LCSMO substrate.

generated by evaluation functions contains the optimum solution. Table 1 lists the optimum solutions that depict the information of film material and the film thickness of each layer. Although the total number of film layers is set as 10, the calculated results only show nine layers with 938 nm thick. This is caused by the film thickness of zero in SAGA.

Fig. 9 shows the simulated spectral reflectivities of the film system at 253 K, 293 K and 333 K. It can be observed that the reflectivity at 253 K is higher than the other temperatures in the far infrared region. This may indicate that the thermal radiation from the LCSMO be reflected by the thin film at the temperature below T_p , thereby the thermal loss is reduced.

Fig. 10 represents the spectral reflectivity of LCSMO and the simulated reflectivity of film system at room temperature. It is noticed that the spectral reflectivity of simulation for the film system is higher than that of pure LCSMO layer in the wavelength range of 0.25–2.5 μm . The simulated average reflectivity of film system is 0.76 in 0.5–2.0 μm region and 0.13 in 2.5–20 μm region. According to Eq. (5), a high reflectivity implies a low solar absorptivity. The simulated solar absorptivity α_s of film system is 0.21, which is very close to the target value 0.2. For an infrared-transparent structure, its absorption loss is very low; and accordingly, the transmissivity of film

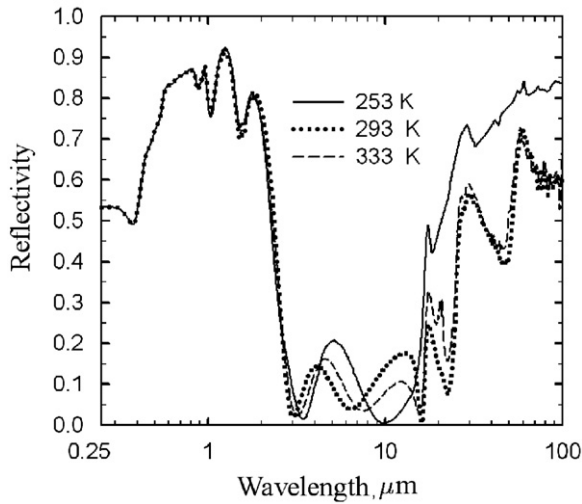


Fig. 9. The calculated spectral reflectivity of film system at 253 K, 293 K and 333 K.

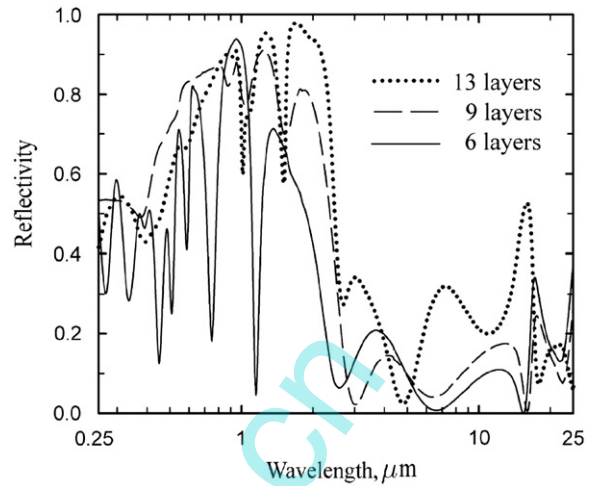


Fig. 11. The simulated spectral reflectivity of film system with different film layers in SAGA.

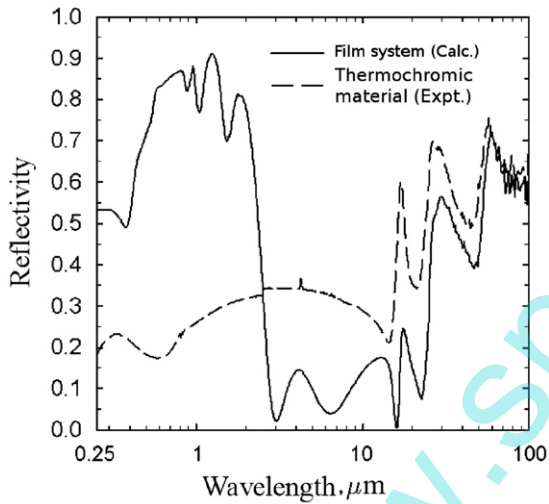


Fig. 10. Reflectivity curve of LCSMO and film system. Solid line denotes film system which was calculated by SAGA; broken line denotes substrate LCSMO which was measured by experiment.

system here can be considered as 0.87 over the wavelength range of 2.5–20 μm . This result indicates that the infrared radiation from LCSMO can penetrate the thin film with low loss. In the far infrared region, three intrinsic reflection peaks of LCSMO do not have much changes, though the optical thin film is coated on the surface of LCSMO.

The effect of number of film layer on the simulated spectral reflectivity is represented as Fig. 11. For the thin film of six layers, the film materials contain the MgF_2 , Ge, and ZnSe. In 0.25–2.5 μm region, the spectral reflectivity of six layers is lower than that of nine layers. This shows that a small number of film layers is not enough to decrease the solar absorptivity to a desired value. In 2.5–25 μm region, the spectral reflectivity of 13 layers is higher than that of nine layers. It is noticed that a large

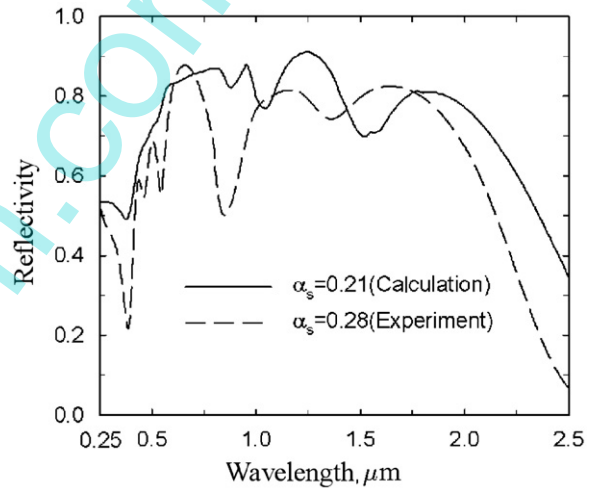


Fig. 12. Reflectivity and solar absorptivity of film system. Solid line denotes the calculation value using SAGA; broken line denotes the experiment value.

number of film layers is hard to ensure a transparent structure. Therefore, the thin film of nine layers successfully satisfy the requirement.

According to the above designed structure, we deposited a thin film on the surface of LCSMO by electron beam evaporation. Fig. 12 shows the simulated and measured reflectivity and solar absorptivity of the film system in 0.25–2.5 μm region. A small mismatch between the measured spectral reflectivity and the calculated one is discovered. The measured spectral reflectivity has a blue shift compared to the calculated value, which may be caused by the error of optical constant of the film material [8]. The strong absorption at 0.36 μm may be due to the introduction of silicon, which has a absorption at the wavelength region from 0.25–0.37 μm . The difference of calculated and measured results at 0.36 μm is attributed to the change of optical constant of Si in the evaporation process. Furthermore, the error of film thickness of each

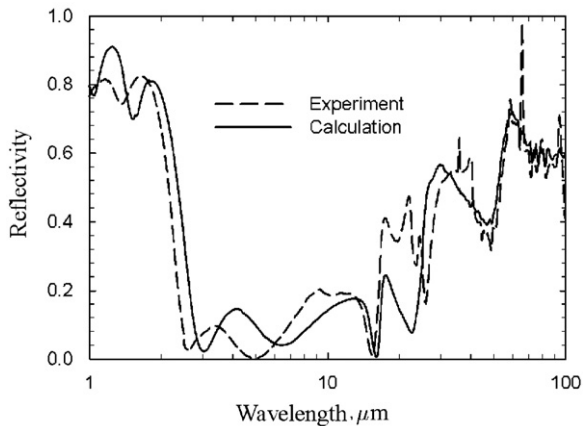


Fig. 13. The results of experiment and calculation of reflectivity of film system.

layer is also an influence factor of mismatch because the thickness has the same order of magnitude as the wavelength. However, experimental results indicates that the solar absorptivity of LCSMO can be reduced experimentally from 0.78 to 0.28 with optical thin film on its surface. Both measured and calculated reflectivity of the film system in the wavelength range of 1–100 μm is illustrated in Fig. 13. Similar blue shift is found in the wavelength region of 2.5–17 μm . The strong absorptions at 22 μm and 46 μm can be attributed to the introduction of MgF_2 , which has a strong absorption around 22 μm and 45 μm , respectively. Comparing with the calculation value, the positions of absorption at 22 μm and 46 μm exhibit a red shift in experiment. For such a phenomenon, during the process of thin film deposition, the optical constant of MgF_2 is influenced, and the MgF_2 material in film system is not ideally isotropic but anisotropic. In spite of the deviation discussed above, the simulated and experimental curves match pretty well in a global view. This results suggest that the solar absorptivity of LCSMO can be reduced successfully by integrating optical thin film on its surface.

7. Conclusions

In this work, the optical properties of $\text{La}_{0.7}\text{Ca}_{0.2}\text{Sr}_{0.1}\text{MnO}_3$ are investigated. In order to reduce its high solar absorptivity, a simulated annealing genetic algorithm is applied to develop a film system, which contains the thin film of nine layers with 938 nm thick and a LCSMO substrate. The thin film is deposited experimentally on the surface of LCSMO by electron beam evaporation. Experiment results show that the solar absorptivity of film system is much less than that of

pure LCSMO. It is suggested that the thin film relax the restriction of LCSMO on the space application.

Acknowledgments

The authors are grateful to Z.M. Huang for his help in the ellipsometry. This work is sponsored by the National Science Foundation of China (Grant nos. 50936002 and 50876044).

References

- [1] Dillon R, Le K, Ianno N. Thermochromic VO_2 sputtered by control of a vanadium–oxygen emission ratio. *Thin Solid Films* 2001;398: 10–6.
- [2] Laffez P, Zaghrioui M, Reversat L, Ruello P. Electron doped $\text{Sm}_{1-x}\text{Ca}_x\text{MnO}_3$ perovskite manganite as potential infrared thermochromic switch. *Appl Phys Lett* 2006;89 081909(1–3).
- [3] Shimazaki K, Tachikawa S, Ohnishi A, Nagasaka Y. Temperature dependence of total hemispherical emittance in perovskite-type manganese oxides, $\text{La}_{1-x}\text{Sr}_x\text{MnO}_3$. *High Temp–High Pressures* 2001;33:525–31.
- [4] Tang G, Yu Y, Chen W, Cao Y. The electrical resistivity and thermal infrared properties of $\text{La}_{1-x}\text{Sr}_x\text{MnO}_3$ compounds. *J Alloys Compd* 2008;461:486–9.
- [5] Li Q, Kuang L, Xuan Y. Prepared method and radiative properties of a thermochromic variable emittance materials. *J Eng Thermophys* 2009;30:1005–8 [in Chinese].
- [6] Siegel R, Hoewll JR. *Thermal radiation heat transfer*. 3rd ed. New York: McGraw-Hill; 1992.
- [7] Macleod HA. *Thin-film optical filters*. 3rd ed. Institute of Physics Publishing; 2001.
- [8] Shimazaki K, Ohnishi A, Nagasaka Y. Development of spectral selective multilayer film for a variable emittance device and its radiation properties measurements. *Int J Thermophys* 2003;24: 757–69.
- [9] Mecherikunnel A, Duncan CH. Total and spectral solar irradiance measured at ground surface. *Appl Opt* 1982;21:554–6.
- [10] Shimazaki K, Tachikawa S, Ohnishi A, Nagasaka Y. Radiative and optical properties of $\text{La}_{1-x}\text{Sr}_x\text{MnO}_3$ ($0 < x < 0.4$) in the vicinity of metal–insulator transition temperatures from 173 to 413 K. *Int J Thermophys* 2001;22:1549–61.
- [11] Srinivas M, Patnaik LM. Adaptive probabilities of crossover and mutation in genetic algorithms. *IEEE Trans Syst Man Cybern A* 1994;24:656–67.
- [12] Eisenhammer T, Lazarov M, Leutbecher M, Schaffel U, Sizmann R. Optimization of interference filters with genetic algorithms applied to silver-based heat mirrors. *Appl Opt* 1993;32:6310–5.
- [13] Martin S, Rivory J, Schoenauer M. Synthesis of optical multilayer systems using genetic algorithms. *Appl Opt* 1995;34:2247–54.
- [14] Shimazaki K, Ohnishi A, Nagasaka Y. Computational design of solar reflection and far-infrared transmission films for a variable emittance device. *Appl Opt* 2003;42:1360–6.
- [15] Hwang SF, He RS. Improving real-parameter genetic algorithm with simulated annealing for engineering problems. *Adv Eng Software* 2006;37:406–18.
- [16] Palik ED. *Handbook of optical constants of solids*. 1st ed. New York: Academic Press; 1985.
- [17] Palik ED. *Handbook of optical constants of solids*. 2nd ed. New York: Academic Press; 1991.
- [18] Jeong IK, Lee JJ. Adaptive simulated annealing genetic algorithm for system identification. *Eng Appl Artif Intel* 1996;9:523–32.